

Stability improvement of $\text{CH}_3\text{NH}_3\text{PbI}_3$ hybrid perovskite through tin and chlorine doping

B. Aguilar, T.E. Soto, K. Sánchez, O. Navarro, A. Valdespino, and D.Y. Torres-Martínez

Unidad Morelia del Instituto de Investigaciones en Materiales, Universidad Nacional Autónoma de México, Antigua Carretera a Pátzcuaro No. 8701, Col. Ex Hacienda de San José de la Huerta, 58190 Morelia, Michoacán, México. e-mails: baguilar@iim.unam.mx; navarro@unam.mx

Received 28 January 2023; accepted 12 April 2023

In recent years, the hybrid perovskite $\text{CH}_3\text{NH}_3\text{PbI}_3$ has been widely studied because of its potential application in the fabrication of high efficiency solar cells. The main challenge is to avoid destabilization of this compound under working conditions. Indeed, the MAPbI_3 begins to decompose into the precursor phases, a few hours or days after being formed. We reported a stability monitoring of doped compounds $\text{CH}_3\text{NH}_3\text{Pb}_{0.9}\text{Sn}_{0.1}\text{I}_{2.8}\text{Cl}_{0.2}$ and $\text{CH}_3\text{NH}_3\text{Pb}_{0.75}\text{Sn}_{0.25}\text{I}_{2.5}\text{Cl}_{0.5}$ obtained as films from solutions of the precursors in N-N dimethylformamide on chemically treated glass substrates. The monitoring was carried out using X-Ray diffraction and absorbance measurements in the UV-Vis region. The tetragonal symmetry initially determined for the three compounds, remains almost unaltered for $\text{CH}_3\text{NH}_3\text{Pb}_{0.75}\text{Sn}_{0.25}\text{I}_{2.5}\text{Cl}_{0.5}$ even after 600 days, under environmental conditions. The bandgap value for this doped perovskite is 1.44 eV.

Keywords: Hybrid perovskites; stability; doping; photovoltaic cells; bandgap.

DOI: <https://doi.org/10.31349/RevMexFis.69.051602>

1. Introduction

The hybrid compounds type perovskite ABX_3 are composed by an organic cation (A), an inorganic cation (B), and a halide (X). The most common ions used are: methylammonium (MA) as the organic cation, Pb as the inorganic cation and I as the halide. The crystalline structure of MAPbI_3 is based on an octahedral PbI_6 configuration, where the Pb atoms stay at the central position and I atoms occupy the vertices of the octahedron, while the methylammonium ions stand at the free spaces between successive octahedra [1]. The polarity of methylammonium and its interaction with inorganic network give to MAPbI_3 unique electronic and optical properties, being widely studied because of its high potential as a semiconductor. The properties like high optical absorption over a broad solar spectrum, high carrier mobility and long carrier lifetime [2–5] make this material highly attractive. These properties, together with low-cost and low temperature production methods have promoted the development and improvement of solar cells based on this material.

Indeed, since 2009, experimental solar cells based on hybrid organic-inorganic-perovskites were fabricated, achieving efficiencies from 3.8% [1] to above of 25% [6]. Nevertheless, the hybrid perovskites degradation has been reported within a few days or hours in operation under standard conditions [7, 8], which is immediately detected by X-ray diffraction (XRD) through a drop in the (100) reflection, in case of MAPbI_3 [9]. The main causes of degradation are photoreduction due to UV light (from the Sun), plus the high reactivity with environmental humidity [10, 11]. The perovskite degradation is due to the hydrophilicity and volatility of the organic cation. Additionally, UV radiation and oxygen can

deteriorate the device performance [12]. To reduce the instability in MAPbI_3 , the iodine as well as lead can be partially replaced by chlorine and tin, respectively [12–15]. Indeed, depending on the halide used, the bandgap can be continuously tuned from 1.6 eV (pure I) to 3.2 eV (pure Cl). The chlorine drives the crystallization dynamics, with a preferential order induced during the crystallization process [16] and more uniform and dense thin films are obtained, giving more chemical stability. Additionally, Cl improves morphology increasing the charge transport [13] due to higher electronegativity [17]. To balance the increased bandgap value caused by chlorine, lead can be partially replaced with tin which reduces the bandgap (until 1.3 eV). It has been reported that the smaller bandgap materials provide the better solar cell efficiencies [11, 16, 18, 19], being 1.75 eV considered ideal [20, 21].

The preparation method is fundamental to achieve the ideal thickness of the perovskite film (about 500 nm), and the crystalline structure. Reported methods start from the same precursors: methylammonium Iodide (MAI) and lead iodide (PbI_6). Most of the bibliography reports the obtention method in two steps: first a layer of PbI_6 is deposited on the substrate and then the MAI is deposited on the PbI_6 by evaporation [22]. Nevertheless, the $\text{CH}_3\text{NH}_3\text{PbI}_3$ perovskite formed by vapor deposition can involve unexpected chemical reactions and competing processes [15]. In a previous work, we obtained thin films of MAPbI_3 by deposition, in one step, of a 1 molar solution containing both precursors, MAI and PbI_6 in N-N-dimethylformamide [23].

In this work, we reported the synthesis and characterization of the doped hybrid perovskites, $\text{CH}_3\text{NH}_3\text{Pb}_{0.9}\text{Sn}_{0.1}\text{I}_{2.8}\text{Cl}_{0.2}$ and $\text{CH}_3\text{NH}_3\text{Pb}_{0.75}\text{Sn}_{0.25}\text{I}_{2.5}\text{Cl}_{0.5}$. Stands

out the improvement of stability under environmental conditions.

2. Methodology

The hybrid perovskites $\text{CH}_3\text{NH}_3\text{Pb}_{0.9}\text{Sn}_{0.1}\text{I}_{2.8}\text{Cl}_{0.2}$ and $\text{CH}_3\text{NH}_3\text{Pb}_{0.75}\text{Sn}_{0.25}\text{I}_{2.5}\text{Cl}_{0.5}$, were synthesized at environmental conditions, 25°C and 45% of humidity. The thin films were obtained from precursor solutions, prepared with methylammonium iodide $\text{CH}_3\text{NH}_3\text{I}$ (98% purity), lead (II) iodide PbI_2 (99% purity) and N-N-dimethylformamide, $(\text{CH}_3)_2\text{N-CHO}$, (99.8% purity), provided by Sigma-Aldrich, and di-hydrated tin chloride, $\text{SnCl}_2 \cdot 2\text{H}_2\text{O}$, provided by Golden-Bell reactants. For each sample, a 1 molar solution was prepared with stoichiometric quantities of the reactants under magnetic stirring at 70°C for 40 minutes [13, 24, 25], which was used as the coating solution onto 1 in^2 glass substrates previously cleaned and chemically attacked.

The chemical attack involves three main steps, first the substrates are cleaned with soap phosphates free and water. They are then placed in a coplin box filled with a chromic solution. After 24 hours, the substrates are rinsed with distilled water until no acid signal is detected. Finally, the substrates are immersed in a nitric acid solution, which is boiled for 3 hours. Once the solution is cold, the substrates are finally rinsed with distilled water then with ethanol. They are stored in ethanol.

The perovskite thin films were obtained from $100 \mu\text{L}$ of precursor solution by using a spin coater at 6000 rpm for 20 s. Solutions and glass substrates were heated at 70°C before deposition. The films were sintered at 140°C for 2 minutes in air to form the perovskites [26].

A low-temperature annealing process ($< 150^\circ\text{C}$) is recommended to help and improve the increases of crystallinity, film morphology, and device performance [11]. At annealing temperatures close to 200°C , perovskite crystals $\text{CH}_3\text{NH}_3\text{PbI}_3$ melt result in lower energy conversion efficiency [27]. According to our observations, varying speed and deposition time, a high velocity of deposition for 2 minutes, assures a low quantity of pinholes over the film. Actually, at an annealing temperature of 100°C , as was reported by some authors [28,29], the perovskite crystals are separated from each other [27], hindering the charge transport.

The crystallinity of perovskite thin films was studied by XRD with a Bruker X-ray diffractometer with $\text{CuK}\alpha$ radiation (1.5418 \AA). The thickness of the perovskite thin films was determined by using a JEOL (JSM-IT300) scanning electron microscope (SEM). The transmission and absorbance spectra were obtained in a Thermo Scientific GENESYS 10S UV-Vis spectrophotometer.

3. Results

In this section, the results for representative samples are presented. In Fig. 1, we can see the elaboration process, the



FIGURE 1. Elaboration process of thin films.

yellow solution containing precursors was deposited in one step on the substrate previously heated. After 2 minutes of sinterization a gray color thin film of hybrid perovskite was obtained.

The stability of thin films of $\text{CH}_3\text{NH}_3\text{Pb}_{0.9}\text{Sn}_{0.1}\text{I}_{2.8}\text{Cl}_{0.2}$ and $\text{CH}_3\text{NH}_3\text{Pb}_{0.75}\text{Sn}_{0.25}\text{I}_{2.5}\text{Cl}_{0.5}$ hybrid perovskites were monitored through XRD and absorbance measurements. Meanwhile, thin films were kept in a Petri dish under environmental conditions. The stable phase of $\text{CH}_3\text{NH}_3\text{PbI}_3$ normally displays eight diffraction peaks: (110), (200), (211), (202), (004), (220), (310) and (224) corresponding to a tetragonal symmetry [1, 12, 30–33], as we see in Fig. 2.

The diffractogram of non-doped perovskite displays the PbI_2 characteristic peak (001) from day 18, whose intensity increases with time indicating a degradation process [23]. The diffractograms obtained for doped perovskites are shown in Fig. 3, where we can see that the hybrid perovskite $\text{CH}_3\text{NH}_3\text{Pb}_{0.9}\text{Sn}_{0.1}\text{I}_{2.8}\text{Cl}_{0.2}$ remains almost unchanged until day 35 [Fig. 3a)]. Also, the incipient PbI_2 peak is observed with no significant later increase. In contrast, hybrid perovskite $\text{CH}_3\text{NH}_3\text{Pb}_{0.75}\text{Sn}_{0.25}\text{I}_{2.5}\text{Cl}_{0.5}$ kept almost unchanged for 20 months, as it is shown in Fig. 3b).

The absorbance spectrum of thin films in the UV-Vis region (400-1100 nm) are showed in Fig. 4. The optical response was monitored until the degradation of hybrid perovskite thin films. An abrupt absorption edge is normally displayed around 780 nm, characteristic of hybrid perovskite

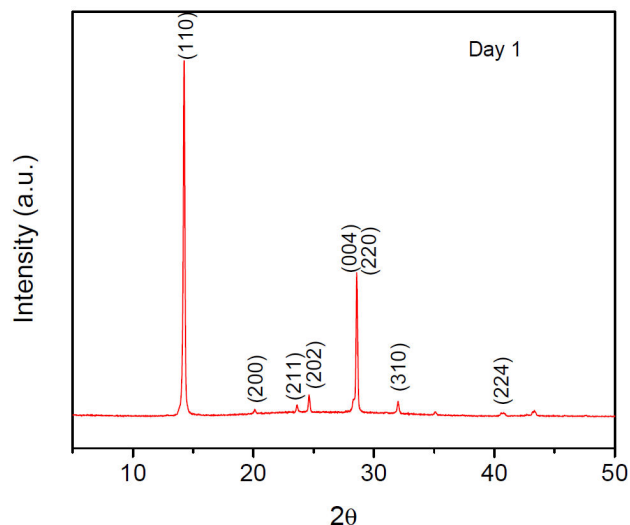


FIGURE 2. Diffractogram of hybrid perovskite $\text{CH}_3\text{NH}_3\text{PbI}_3$ (MAPI).

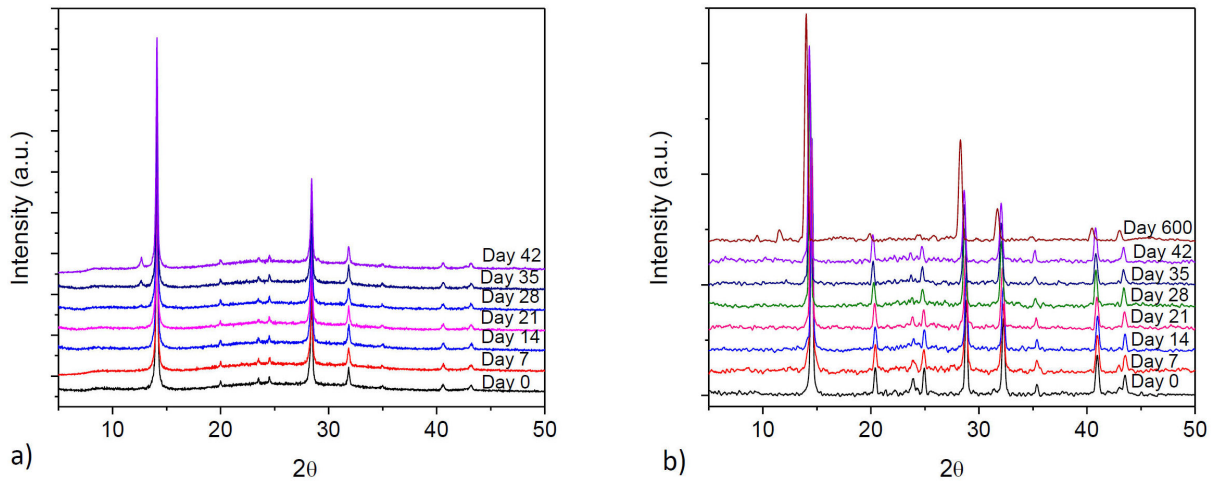


FIGURE 3. DRX of a) sample of doped perovskite $\text{CH}_3\text{NH}_3\text{Pb}_{0.9}\text{Sn}_{0.1}\text{I}_{2.8}\text{Cl}_{0.2}$, no degradation peak is present until 35 days, b) doped perovskite $\text{CH}_3\text{NH}_3\text{Pb}_{0.75}\text{Sn}_{0.25}\text{I}_{2.5}\text{Cl}_{0.5}$, showing the degradation peak after 600 days.

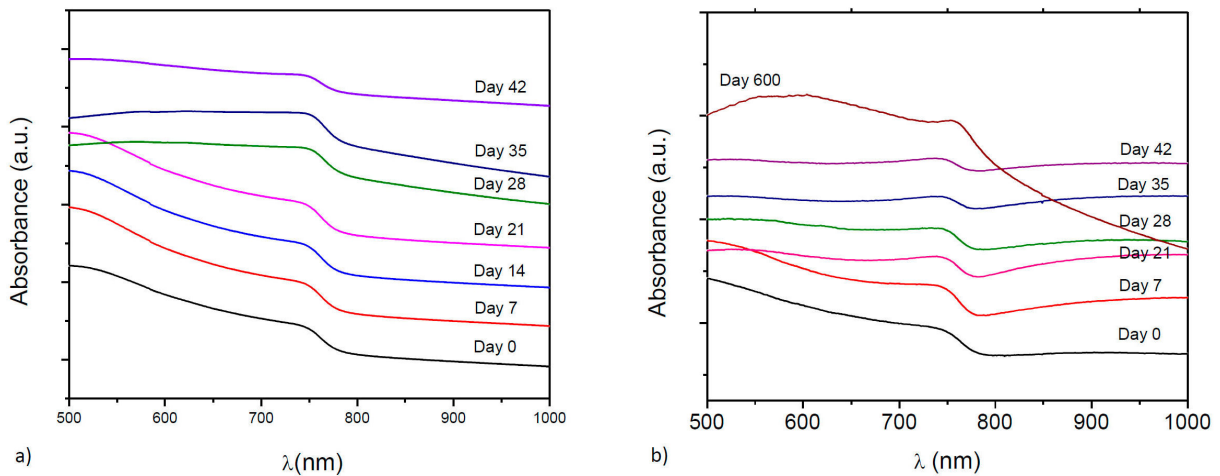


FIGURE 4. Absorbance versus Energy for a) $\text{CH}_3\text{NH}_3\text{Pb}_{0.9}\text{Sn}_{0.1}\text{I}_{2.8}\text{Cl}_{0.2}$ and b) $\text{CH}_3\text{NH}_3\text{Pb}_{0.75}\text{Sn}_{0.25}\text{I}_{2.5}\text{Cl}_{0.5}$.

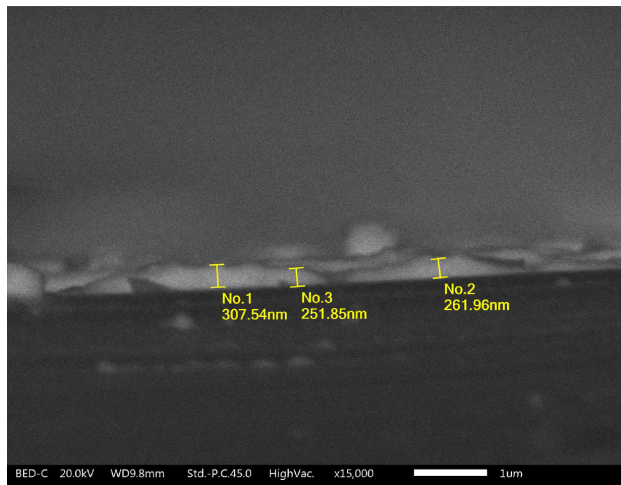


FIGURE 5. Thickness determined through SEM observations for $\text{CH}_3\text{NH}_3\text{Pb}_{0.75}\text{Sn}_{0.25}\text{I}_{2.5}\text{Cl}_{0.5}$.

[34, 35], which corresponds to the direct gap transition from the first valence band to the conduction band minimum. For doped hybrid perovskites we see the same behavior, indicating that doping does not significantly change the optical properties, [Figs. 4a) and 4b)]. We used the Tauc equation to calculate the optical bandgap value, E_g [25, 26], for a direct bandgap semiconductor: $(\alpha h\nu)^2 = A(h\nu - E_g)$. The absorption coefficient α of the film was calculated by using $\alpha = (2.302[A/d])$ from the absorbance spectrum and the thickness of the films, d [15, 22, 35]. This later is obtained from SEM observations of cross section, being of around 300 nm, as we can see in Fig. 5.

The photon energy, $h\nu$, is determined by extrapolation of the linear portion of the curve obtained by plotting $(\alpha h\nu)^2$ versus $h\nu$, until the intercept with the photon energy axis (Fig. 6). The bandgap value is $E_g = 1.56$ eV for $\text{CH}_3\text{NH}_3\text{Pb}_{0.9}\text{Sn}_{0.1}\text{I}_{2.8}\text{Cl}_{0.2}$ [Fig. 6a)] and 1.43 eV for

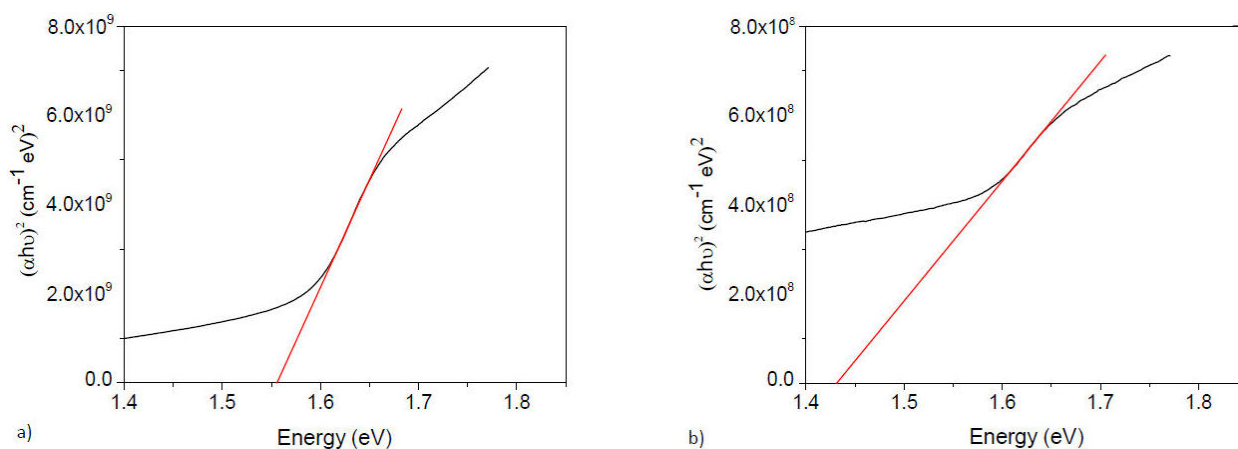


FIGURE 6. Extrapolation of the linear portion of $(\alpha h\nu)^2$ versus $h\nu$, to find the bandgap value for a) $\text{CH}_3\text{NH}_3\text{Pb}_{0.9}\text{Sn}_{0.1}\text{I}_{2.8}\text{Cl}_{0.2}$ and b) $\text{CH}_3\text{NH}_3\text{Pb}_{0.75}\text{Sn}_{0.25}\text{I}_{2.5}\text{Cl}_{0.5}$.

$\text{CH}_3\text{NH}_3\text{Pb}_{0.75}\text{Sn}_{0.25}\text{I}_{2.5}\text{Cl}_{0.5}$ [Fig. 6b)] thin films. These values are very close to 1.54 eV corresponding to $\text{CH}_3\text{NH}_3\text{PbI}_3$, within ideal range previously reported [20, 22, 23, 36].

4. Conclusions

In summary, we have reported the stability improvement of the $\text{CH}_3\text{NH}_3\text{PbI}_3$ hybrid perovskite by doping with tin and chlorine. The bandgap obtained from UV-Vis measurements for the doped hybrid perovskites confirm that controlled dop-

ing leaves us to obtain a more stable compound with non-significant changes. This is due to the fact of chlorine stabilizes the structure with an increase of bandgap, which is compensated with the introduction of tin that decreases the bandgap.

Acknowledgments

This work was partially supported by grant PAPIIT IN108422 from UNAM México. One of us, T.E. Soto, thanks to CONACYT for the scholarship No. I1200/94/2020.

1. A. Kojima, K. Teshima, Y. Shirai, T. Miyasaka, Organometal Halide Perovskites as Visible-Light Sensitizers for Photovoltaic Cells, *J. Am. Chem. Soc.* **131** (2009) 2024.
2. J.-H. Im, J. Chung, S.-J. Kim, N.-G. Park, Synthesis, structure, and photovoltaic property of a nanocrystalline 2H perovskite-type novel sensitizer $\text{CH}_3\text{CH}_2\text{NH}_3\text{PbI}_3$, *Nanoscale Research Letters* **7** (2012) 353.
3. F. Deschler *et al.*, High Photoluminescence Efficiency and Optically Pumped Lasing in Solution-Processed Mixed Halide Perovskite Semiconductors, *J. Phys. Chem. Lett.* **5** (2014) 1421.
4. L. E. Polander, P. Pahnner, M. Schwarze, M. Saalfrank, C. Koenner, K. Leo, Hole-transport material variation in fully vacuum deposited perovskite solar cells, *APL Materials*. **2** (2014) 081503.
5. W.E.I. Sha, X. Ren, L. Chen, W.C.H. Choy, The efficiency limit of $\text{CH}_3\text{NH}_3\text{PbI}_3$ perovskite solar cells, *Appl. Phys. Lett.* **106** (2015) 221104.
6. R. Pandey *et al.*, Mutual Insight on Ferroelectrics and Hybrid Halide Perovskites: A Platform for Future Multifunctional Energy Conversion, *Adv. Mater.* **31** (2019) 1807376.
7. R.F. Service, Perovskite solar cells gear up to go commercial, *Science*. **354** (2016) 1214.
8. L. Lanzetta *et al.*, *Nature Comm.* **12** (2021) 2853.
9. H. Syafutra *et al.*, *Nanomaterial*. **10** (2020)1254.
10. A. Kakekhani, R. N. Katti, A. M. Rappe, Water in hybrid perovskites: Bulk MAPbI_3 degradation via super-hydrous state, *APL Mater.* **7** (2019) 041112.
11. A. Polman, M. Knight, E.C. Garnett, B. Ehrler, W.C. Sinke, Photovoltaic materials: Present efficiencies and future challenges, *Science*. **352** (2016) 6283.
12. G. Grancini *et al.*, The Impact of the Crystallization Processes on the Structural and Optical Properties of Hybrid Perovskite Films for Photovoltaics, *J. Phys. Chem. Lett.* **5** (2014) 3836.
13. D.W. DeQuilettes *et al.*, Impact of microstructure on local carrier lifetime in perovskite solar cells, *Science*. **348** (2015) 6235.
14. A.H. Ip *et al.*, A two-step route to planar perovskite cells exhibiting reduced hysteresis, *Appl. Phys. Lett.* **106** (2015) 143902.
15. S. Yuan, Z. Qiu, H. Zhang, H. Gong, Y. Hao, B. Cao, Oxygen influencing the photocarriers lifetime of $\text{CH}_3\text{NH}_3\text{PbI}_{3-x}\text{Cl}_x$ film grown by two-step interdiffusion method and its photovoltaic performance, *Appl. Phys. Lett.* **108** (2016) 033904.
16. N. K. Kumawat, A. Dey, K. L. Narasimhan, D. Kabra, Near Infrared to Visible Electroluminescent Diodes Based on Organometallic Halide Perovskites: Structural and Optical Investigation, *ACS Photonics*. **2** (2015) 349.

17. F. El-Mellouhi, A. Marzouk, E. T. Bentría, S. N. Rashkeev, S. Kais, F. H. Alharbi, Hydrogen Bonding and Stability of Hybrid Organic-Inorganic Perovskites, *Chem. Sus. Chem.* **9** (2016) 2648.
18. O. Granas, D. Vinichenko, E. Kaxiras, Establishing the limits of efficiency of perovskite solar cells from first principles modeling, *Nature Scientific Reports* **6** (2016) 36108.
19. S.N. Habisreutinger, D.P. McMeekin, H.J. Snaith, R.J. Nicholas, Research Update: Strategies for improving the stability of perovskite solar cells, *Apl. Mater.* **4** (2016) 091503.
20. G.E. Eperon *et al.*, Perovskite-perovskite tandem photovoltaics with optimized band gaps, *Science*. **354** (2016) 6314.
21. D.P. McMeekin *et al.*, A mixed-cation lead mixed-halide perovskite absorber for tandem solar cells, *Science*. **351** (2016) 6269.
22. L. Liu, J.A. McLeod, R. Wang, P. Shen, S. Duhm, Tracking the formation of methylammonium lead triiodide perovskite, *Appl. Phys. Lett.* **107** (2015) 061904.
23. D. Y. Torres-Martinez, M. Millán, B. Aguilar, O. Navarro, Synthesis and characterization of CH₃NH₃PbI₃ perovskite thin films obtained in one step, *Physica B*. **585** (2020) 412081.
24. Q.-K. Wang *et al.*, Energy Level Offsets at Lead Halide Perovskite/Organic Hybrid Interfaces and Their Impacts on Charge Separation, *Adv. Mater. Interfaces*. **2** (2015) 1400528.
25. M.I. Saidaminov *et al.*, High-quality bulk hybrid perovskite single crystals within minutes by inverse temperature crystallization, *Nat. Commun.* **6** (2015) 7586.
26. X. Song, W. Wang, P. Sun, W. Ma, Z. Chen, Additive to regulate the perovskite crystal film growth in planar heterojunction solar cells, *Appl. Phys. Lett.* **106** (2015) 033901.
27. B.E. Cohen, S. Gamliel, L. Etgar, Parameters influencing the deposition of methylammonium lead halide iodide in hole conductor free perovskite-based solar cells, *Apl. Mater.* **2** (2014) 081502.
28. X. Li, D. Bi, Ch Yi, J.-D. Dcoppet, J. Luo, S.M. Zakeeruddin, A. Hagfeldt, M. Gratzel, A vacuum flash-assisted solution process for high-efficiency large-area perovskite solar cells, *Science*. **353** (2016) 6294.
29. R.G. Niemann *et al.*, Halogen Effects on Ordering and Bonding of CH₃NH₃⁺ in CH₃NH₃PbX₃ (X = Cl, Br, I) Hybrid Perovskites: A Vibrational Spectroscopic Study, *J. Phys. Chem. C* **120** (2016) 2509.
30. W. Nie *et al.*, High-efficiency solution-processed perovskite solar cells with millimeter-scale grains, *Science*. **347** (2015) 6221.
31. J. Ding *et al.*, High-quality inorganic-organic perovskite CH₃CH₂NH₃PbI₃ single crystals for photo-detector applications, *J. Mater. Sci.* **52** (2017) 276.
32. E. Guangqing Tai, R. T. Wang, J. Y. Chen, G. Xu, A Water-Stable Organic-Inorganic Hybrid Perovskite for Solar Cells by Inorganic Passivation, *Crystals*. **9** (2019) 83.
33. S.K. Ojha, A. Singh, A. Ojha, Modifications in structural morphology of CH₃CH₂NH₃PbI₃ perovskite using nitrilotriacetic acid and glycine as habit modifiers, *Mater. Chem. Phys.* **240** (2020) 122149.
34. M. DeBastiani, V.D. Innocenzo, S.D. Stranks, H.J. Snaith, A. Petrozza, Role of the crystallization substrate on the photoluminescence properties of organo-lead mixed halides perovskites, *Apl. Mater.* **2** (2014) 081509.
35. J. Xie, Y. Liu, J. Liu, L. Le, Q. Gao, J. Li, S. Yang, *J. Power Sources*. **28** (2015) 349.
36. D.K. Chaudhary, P. Kumar, L. Kumar, Impact of CH₃CH₂NH₃PbI₃-PCBM bulk heterojunction active layer on the photovoltaic performance of perovskite solar cells, *Chem. Phys. Lett.* **685** (2017) 210.